The Journal of Neuroscience, January 1, 1998, *18*(1):388–398

Gamma Oscillations in the Entorhinal Cortex of the Freely Behaving Rat

J. J. Chrobak and G. Buzsáki

Center for Molecular and Behavioral Neuroscience, Rutgers, The State University of New Jersey, Newark, New Jersey 07102

Gamma frequency field oscillations (40–100 Hz) are nested within theta oscillations in the dentate–hilar and CA1–CA3 regions of the hippocampus during exploratory behaviors. These oscillations reflect synchronized synaptic potentials that entrain the discharge of neuronal populations within the ~10–25 msec range. Using multisite recordings in freely behaving rats, we examined gamma oscillations within the superficial layers (I–III) of the entorhinal cortex. These oscillations increased in amplitude and regularity in association with entorhinal theta waves. Gamma waves showed an amplitude minimum and reversed in phase near the perisomatic region of layer II, indicating that they represent synchronized synaptic potentials impinging on layer II–III neurons. Theta and gamma oscillations in the entorhinal cortex were coupled with theta and gamma oscillations in the dentate hilar region. The majority of layer II–III neurons discharged irregularly but were phase-related to the negative peak of the local (layer II–III) gamma field oscillation. These findings demonstrate that layer II–III neurons discharge in temporally defined gamma windows (~10–25 msec) coupled to the theta cycle. This transient temporal framework, which emerges in both the entorhinal cortex and the hippocampus, may allow spatially distributed subpopulations to form temporally defined ensembles. We speculate that the theta–gamma pattern in the discharge of these neurons is essential for effective neuronal communication and synaptic plasticity in the perforant pathway.

Key words: neuronal cooperativity; unit activity; theta waves; gamma; plasticity; Alzheimer's dementia; perforant pathway; LTP/LTD

"The ultimate physical substrate of memory formation and consolidation resides in alteration in synaptic efficacy, which then alters the patterns of activity in large aggregate collections of cortical neurons" (Hebb, 1949). It is the modifications in the patterns of activity in large aggregate collections of neurons that have relevance to the cognitive operations of the mammalian brain. The means by which large collections of neurons, within and across vast regions of the brain, can effectively interact is not well understood.

The occurrence and transient sychronization of neurons to local field oscillations has been demonstrated in many neural networks (Buzsáki et al., 1983, 1992; Llinás, 1988; Gray, 1989; Steriáde et al., 1990, 1993, 1996; Murthy and Fetz, 1992; Singer, 1993; Freeman and Barrie, 1994; Fregnac et al., 1994; Bragin et al., 1995; Ylinen et al., 1995; Laurent, 1996; Laurent et al., 1996). The local field oscillations reflect synchronized synaptic inputs that determine neuronal discharge. The oscillations, in effect, reflect entrainment mechanisms for timing the discharge of neurons within a local network and, likewise, in interconnected distant networks (Buzsáki and Chrobak, 1995).

Previously, we have described the 200 Hz synchronization of neuronal discharge within CA1, subiculum, and the deep layers of the entorhinal cortex in association with hippocampal sharp waves during consummatory behavior and slow-wave sleep (Buzsáki et al., 1992; Chrobak and Buzsáki, 1994, 1996a,b; Ylinen et al., 1995). The present study describes a different temporal pattern, a gamma (40–100 Hz) oscillation, that occurs within the superficial layers of the entorhinal cortex in association with entorhinal theta waves during exploratory behavior and rapid eye movement (REM) sleep.

Neurons within the superficial layers (II–III) of the entorhinal cortex (EC) provide the neocortical input to the hippocampus (Steward and Scoville, 1976; Witter and Groenewegen, 1984; Amaral and Witter, 1995). Via these neurons, the end product of neocortical associative processes are fed into the circuitry of the hippocampus. Damage to this population of cells is thought to be a clinical precursor to Alzheimer's dementia and likely underlies the mnemonic deficits that characterize the presenting symptoms of that disorder (Hyman et al., 1984; Van Hoesen et al., 1991; Braak and Braak, 1995). Understanding the systems physiology of this cell population should contribute to an understanding of the mechanisms that subserve memory function and dysfunction as instantiated in entorhinal–hippocampal circuits.

Using 16-site silicon probes to record entorhinal field potentials concurrently across the superficial layers of this structure, we demonstrate that oscillatory patterns in the gamma range occur nested within theta cycles and exhibit a phase reversal zone within layer II of the entorhinal cortex. Single-unit recordings by the 16-site probes and single tungsten electrodes were used to demonstrate that individual layer II–III neurons discharge in relation to the local oscillation. Thus, the distributed population

Received Oct. 15, 1996; revised Oct. 3, 1997; accepted Oct. 9, 1997.

This work was supported by the Alzheimer's Association, National Institutes of Health Grants NS34994 and 1P41RR09754, Human Frontier Science Program, and Whitehall Foundation. We thank Heather Read and Anatol Bragin for all their help, comments, and discussion, as well as Kensall Wise and Jamille Hetke for supplying silicon probes.

Correspondence should be addressed to Gyorgy Buzsáki, Center for Molecular and Behavioral Neuroscience, Rutgers University, 197 University Avenue, Newark, NJ 07102.

Dr. Chrobak's present address: Center for Neuroscience, University of California-Davis, 1544 Newton Court, Davis, CA 95616.

output of neurons within the superficial layers of the EC is entrained into a theta–gamma population rhythm.

MATERIALS AND METHODS

Animals and surgery. Nineteen adult Sprague Dawley rats were used in the present experiments. For surgery, rats were anesthetized with a ketamine mixture (4 ml/kg) consisting of (in mg/ml): 25 ketamine, 1.3 xylazine, and 0.25 acepromazine. After a midline scalp incision, two to four burr holes were drilled in the skull over the hippocampal and retrohippocampal cortices. Two or three sets of four 50 μm tungsten wires were positioned into the left and right dorsal hippocampus–subicular regions [anteroposterior (AP), −2.5, −5.0, −7.5 mm from bregma; mediolateral (ML), 1.5, 2.5, 4.0; dorsoventral (DV), 2–4.00 mm from the skull, according to Paxinos and Watson (1986)] and above retrohippocampal regions (AP, −7.5–9.0; ML, 3–5.0). At least one set of hippocampal electrodes, positioned ipsilateral to the retrohippocampal electrodes, was attached to a drive consisting of a brass post and a single machine screw. This allowed for optimal positioning of electrodes in the awake animal. In 15 rats, one or two single tungsten microelectrodes (0.5–3.0 MΩ) mounted to similar drives were positioned over one or two retrohippocampal areas (AP, −7.5–9.0; ML, 3–5.0). These mounts allowed for the slow passage of the microelectrode through the retrohippocampal region. In five additional animals, a 16-site silicon probe (100 μm tip separations) (Wise and Najafi, 1991; Bragin et al., 1995) was positioned via a movable microdrive into the EC. A pair of 150 μm wires was also positioned in the angular bundle (AP, 7.2; ML, 4.2; DV, 4.0) or CA3 region (AP, 4.0; ML, 4.0; DV, 4.0) for stimulation. Two stainless steel watch screws driven into the bone above the cerebellum served as indifferent (reference) and ground electrodes. Two or more additional support screws were positioned, and the entire ensemble was secured to the skull with dental acrylic. All electrodes were attached to male pins that were secured in a rectangular eight by four pin array and secured with dental acrylic.

Recording of field and unit activity. Bioelectrical activity was recorded monopolarly against the reference electrode in freely behaving rats during either movement, awake immobility, or distinct sleep stages. The animal's head stage (male pins) was connected to 24 metal oxide semiconductor field effect transistor input operational amplifiers mounted in a female connector. The amplifiers served to eliminate cable movement artifacts (Buzsáki, 1989). An attached cable fed into a rotating swivel (Biela, Inc., Irvine, CA) allowed for the free rotation of the recording cable and movement of the rodent within a standard Plexiglas home cage or a Plexiglas open field apparatus (50 × 50 cm). An amplifier system (Grass Neurodata Acquisition System, Quincy, MA) and an analog-to-digital hardware–software system (EGAA; RC Electronics, Santa Barbara, CA) run on a personal computer allowed for direct visualization and storage of electrical activity. Wide band signals (1 Hz–0.5, 1, and 5 kHz) were sampled at 1, 2, or typically 10 kHz and stored on optical disks.

After optimization of hippocampal microelectrodes, one or two tungsten microelectrodes or a 16-site silicone probe was lowered through retrohippocampal structures. Discriminable units and/or prominent oscillations were recorded during theta states (locomotor activity and paradoxical sleep) for 30–300 sec epochs. Typically, these epochs were recorded interspersed with recording of hippocampal and entorhinal sharp waves during awake immobility and slow-wave sleep epochs. Some of the data concerning the discharge character of these neurons during these states have been reported previously (Chrobak and Buzsáki, 1994, 1996a). When possible (depending on the stability of unit recording), multiple continuous epochs (30–300 sec) were recorded during both sharp waves as well as during theta. After completion of a single pass of the movable microelectrode(s), which involved intermittent recordings for 1–7 d, rats were anesthetized with pentobarbital and perfused with the electrodes *in situ*.

Data processing and analysis. Unit activity and field potentials were digitally filtered (120 dB/octave: unit, bandpass 0.5–5 kHz; high-frequency oscillations, bandpass 50–150 Hz) and analyzed off-line on a 486 33 MHz and/or an IBM RS 6000 computer. Putative single units (units typically greater than three to five times the baseline amplitude) were verified by the absence of spikes ≥1 msec in autocorrelograms. Thus, amplitude discriminated spikes with refractory periods of >1 msec were considered single units. Remaining unit activity (units less than three times baseline and/or with interspike intervals of <1 msec) were considered multiunit. Gamma peaks were detected after off-line filtering (50–150 Hz) using a peak detection algorithm.

Single-unit and multiunit activity were cross-correlated with local entorhinal gamma peaks to determine the phase relationship between unit activity and the local gamma field oscillation. In all cross-correlograms, the negative peaks of the local entorhinal gamma oscillation served as the zero reference point. Unit activity was considered gamma-modulated if the number of events in a 10 msec time bin (±5 msec from the zero reference) demonstrated at least a 100% increase compared with the 10 msec time bins 45 msec before time 0 and 45 msec after time 0. Furthermore, gamma peaks within the dentate–hilar region were cross-correlated with local entorhinal gamma peaks to determine the synchronization between regions. Local field averages were obtained by averaging wide-band or filtered signals using gamma peaks or unit pulses (spike-triggered averages) as the zero reference. The local field averages illustrate the relationship of the local field EEG to a reference event (i.e., dentate or entorhinal theta in relation to entorhinal gamma oscillations).

Spectral analyses and coherence were assessed from artifact-free EEG segments. Each segment (2.54 sec) was tapered off through a Hamming window and converted by fast Fourier transform. Power spectra were averaged from two or four EEG segments and plotted as a function of frequency and depth. Coherence and phase measurements were calculated from summed values from the spectra 6–12 Hz for theta and 40–120 Hz for gamma. Coherence was calculated for two EEG signals derived from two electrodes on the 16-site probe. The coherence spectrum is a measure of the statistical correlation between these two signals as a function of frequency (Buzsáki et al., 1983; Leung and Buzsáki 1983). Squared coherence, K^2_{xy}, for two signals, x and y, is equal to the average cross-power spectrum normalized by the averaged powers of the individual signals: $K^2_{xy} = [C_{xy}]^2/(C_{xx}\,C_{yy})$. Current source density (CSD) was performed as described previously (Bragin et al., 1995; Ylinen et al., 1995). Although some resistivity differences may be present in the different cortical layers, which may influence the magnitude of sinks and sources, in practice these are not large enough to modify the calculated distribution of current generators significantly. The CSD results are presented as the unscaled second derivative of voltage as a function of depth. The exact anatomical layers corresponding to the vertical scale of the CSD maps were reconstructed with the aid of the histologically identified recording tracks.

Histology. Tissue was processed using either thionin stain or a modified silver method that allows for direct visualization of damaged neurons at the electrode tip (Gallyas et al., 1990). After completion of the experiments the rats were deeply anesthetized and perfused through the heart first with cacodylate-buffered saline, pH 7.5, followed by a cacodylate-buffered fixative containing 4% paraformaldehyde and 5.9% calcium chloride, pH 7.5. Brains were left *in situ* for 24 hr, removed, and then post-fixed in the same solution for 1 week. The brains were sectioned on a vibratome at 80 μm. They were dehydrated with propanol and placed in an esterifying solution (98% propanol and 1.2% sulfuric acid) at 56°C for 16 hr. After rehydration and sectioning they were processed according to the following procedure: (1) pretreatment in 8% acetic acid for 10 min, (2) washing in water for 1 min, (3) physical development with tungstosilicic acid for ~10 min, and (4) washing in 1% acetic acid. Finally, the sections were dehydrated, mounted on slides, and coverslipped.

RESULTS

Entorhinal theta and gamma: oscillatory extracellular field potentials occurring concurrently with hippocampal theta and gamma

Prominent theta oscillations could be observed throughout the EC during exploratory behavior and REM sleep (Fig. 1*A*) that were in phase with hippocampal theta recorded in CA1 stratum oriens and stratum pyramidale. In association with theta, we observed a gamma oscillation that varied between 40 and 100 Hz. The power of gamma activity, as reflected by the area of the power between 40 and 100 Hz, was larger during theta than in its absence in every animal investigated. When long theta and gamma epochs, obtained during exploration (walking, rearing, and sniffing) or during the paradoxical phase of sleep, were subjected to spectral analysis, the increased gamma power was distributed over a wide frequency range. On the other hand, when epochs of similar theta frequency were selected from long

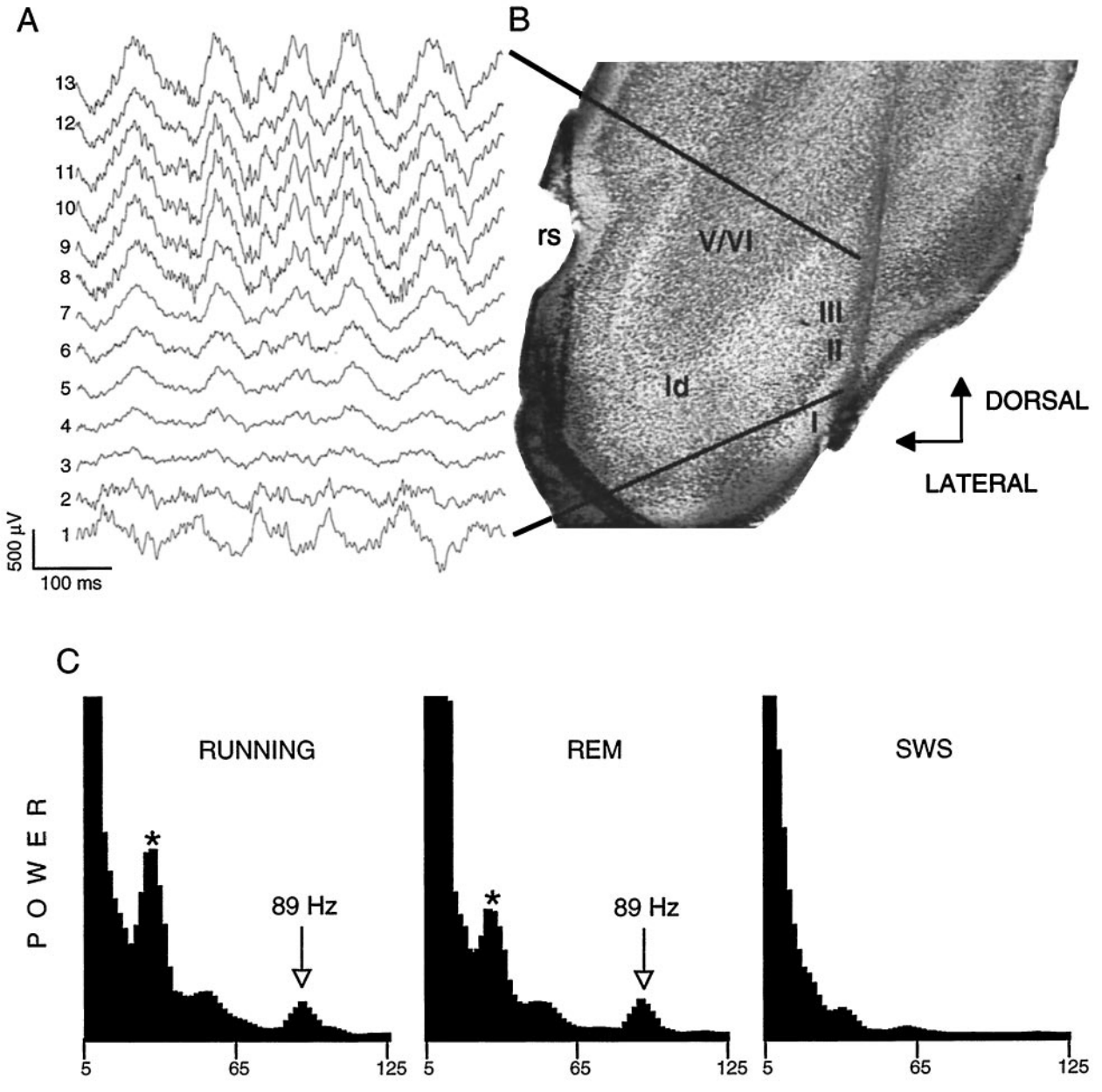

Figure 1. Gamma and theta waves in the entorhinal cortex. *A*, Depth (*left*) profile of entorhinal theta waves. A 16-site silicon probe (13 most ventral sites shown) was used to record field and unit activity concurrently at multiple laminar sites within the entorhinal cortex. The span of the recorded area is indicated by *lines* in *B*. Note the gradual decrease in amplitude and phase shift of theta, which then reverses in phase near the superficial aspect of layer II (compare *trace 1* with *traces 4–13*). *B*, Image (*right*) is a Nissl-stained section illustrating the position of the 16-site recording probe within the superficial layers of the entorhinal cortex. *rs*, Rhinal sulcus; *para*, parasubiculum; *ld*, lamina dissecans; *I–V*, specific lamina. *C*, Power spectra of EEG extracts during different behaviors. Large peaks at theta frequency (8–9 Hz bins) were present during *RUNNING* and *REM* sleep but not during slow wave sleep (*SWS*; these peaks are cut off to emphasize gamma power). The *asterisk* indicates the third harmonic of theta frequency peak (absent during *SWS*). Note similar gamma peaks during *RUNNING* and *REM* sleep and absence of gamma frequency peak during *SWS* episode. The *y*-scale (*POWER*) is linear.

records, prominent peaks were observed in a relatively narrow gamma band (Fig. 1*C*). Faster theta waves were accompanied by faster-frequency gamma peaks in the power spectra, similar to the theta–gamma relationship in the hippocampus (Bragin et al., 1995).

Five animals were implanted with movable 16-site silicon probes to record entorhinal field potentials concurrently across the superficial layers of this structure. In confirmation of previous findings, theta waves showed a phase-shifted dipole in the superficial layers of the EC (Alonso and Garcia-Austt, 1987a; Mitchell and Ranck, 1980) in which layer I theta is 180° phase-shifted compared with layer II–III. Nested within the troughs of layer II–III theta, prominent gamma oscillations could be observed (Figs. 2, 3). The amplitude of gamma activity was largest in layer III. A "null zone" (i.e., amplitude minimum) and phase reversal of gamma waves occurred near the perisomatic region of layer II. The width of the null zone varied according to the relationship between the penetration angle and the cytoarchitecture of the recorded area. In four of the animals, the probe penetrated into layer I, and we observed a polarity reversal of both theta and

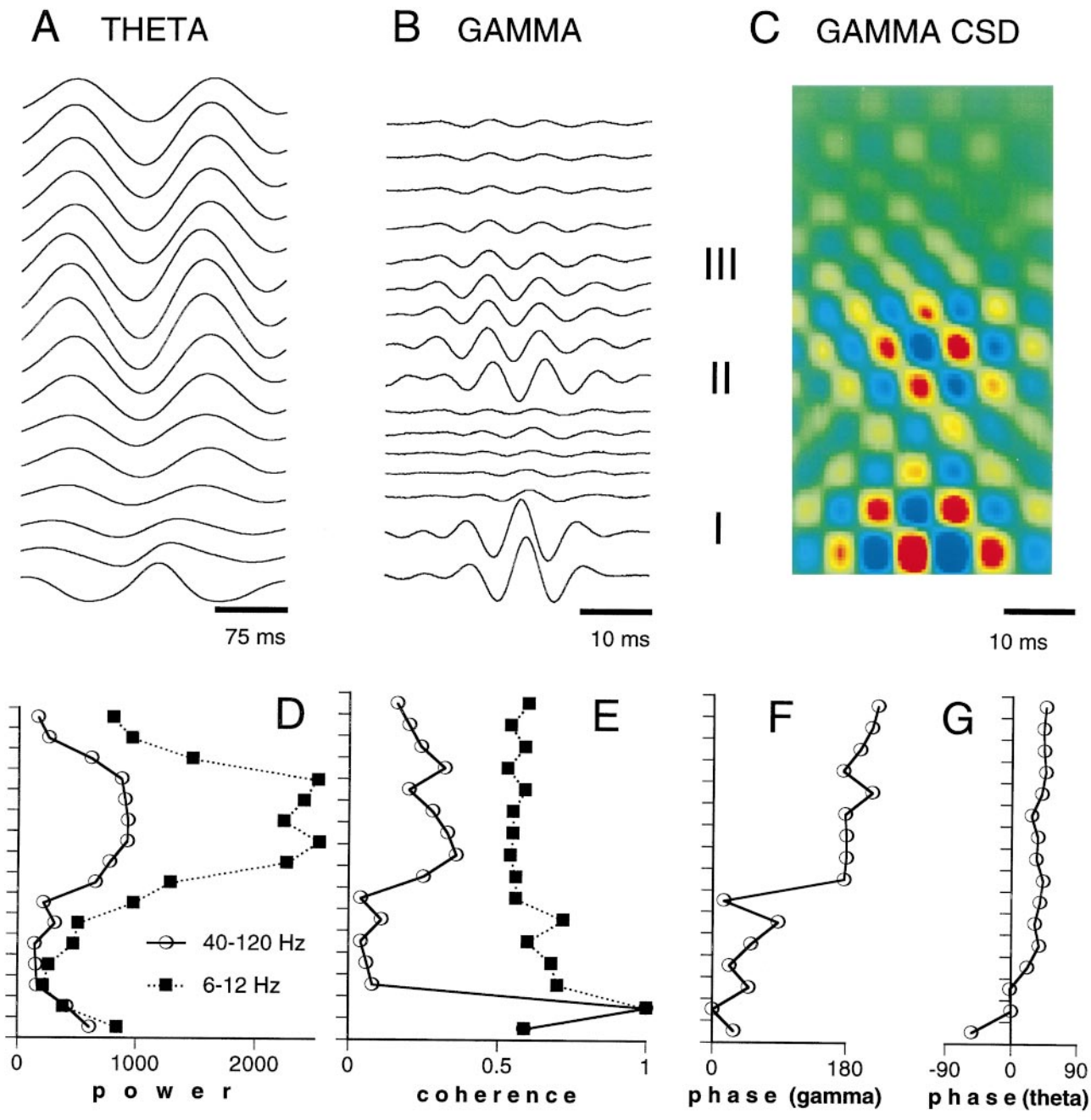

Figure 2. Depth versus amplitude profiles of theta and gamma oscillations in the entorhinal cortex. *A, B*, Averaged extracellular field potentials illustrating theta and gamma oscillations across layers I–III of the entorhinal cortex. The averager was triggered by the positive peaks of filtered (1–20 Hz; 50–150 Hz) waves recorded from site 1 (*bottom trace*). The wide null zone of gamma waves is attributable to the oblique penetration of the recording silicon probe (shown in Fig. 1). *C*, Corresponding current source density analysis of gamma oscillation. *Cold colors*; Sinks; *hot colors*, sources. *D–G*, Laminar distribution of power, coherence, and phases of theta and gamma oscillations. Coherence and phase measurements are relative to site 2 from *bottom*. The values indicate summed values from the spectra from 6 to 12 Hz (theta) and 40 to 120 Hz (gamma). Note phase reversal of gamma oscillation between layers I and II.

gamma waves (Figs. 1–3). In the experiment shown in Figures 1 and 2, the electrode penetrated layers IV–I obliquely (Fig. 1*B*), and several sites recorded in and around layer II and two sites recorded within layer I. As a result, a rather wide reversal zone rather than a reversal "point" was present. In three animals the probe was more or less perpendicular to layer II. In these rats, phase reversal of gamma activity occurred within 100–200 μm (Fig. 3). In the fifth rat, the probe did not penetrate into layer I, and no reversal of theta or gamma phase was observed (see histology in Fig. 5). Spectral analysis of gamma waves along the layer IV–layer I axis of the entorhinal cortex revealed coherence values ranging from 0.2 to 0.5 (Fig. 2).

We also examined the relationship between gamma waves at layer II–III sites and gamma activity at ipsilateral dentate–hilar sites ($n = 8$). Figure 4 illustrates prominent synchrony of gamma patterns between a site in the lateral entorhinal cortex and the dorsal hippocampus. Note the multiple peaks and troughs in the cross-correlogram. This example represents the highest coher-

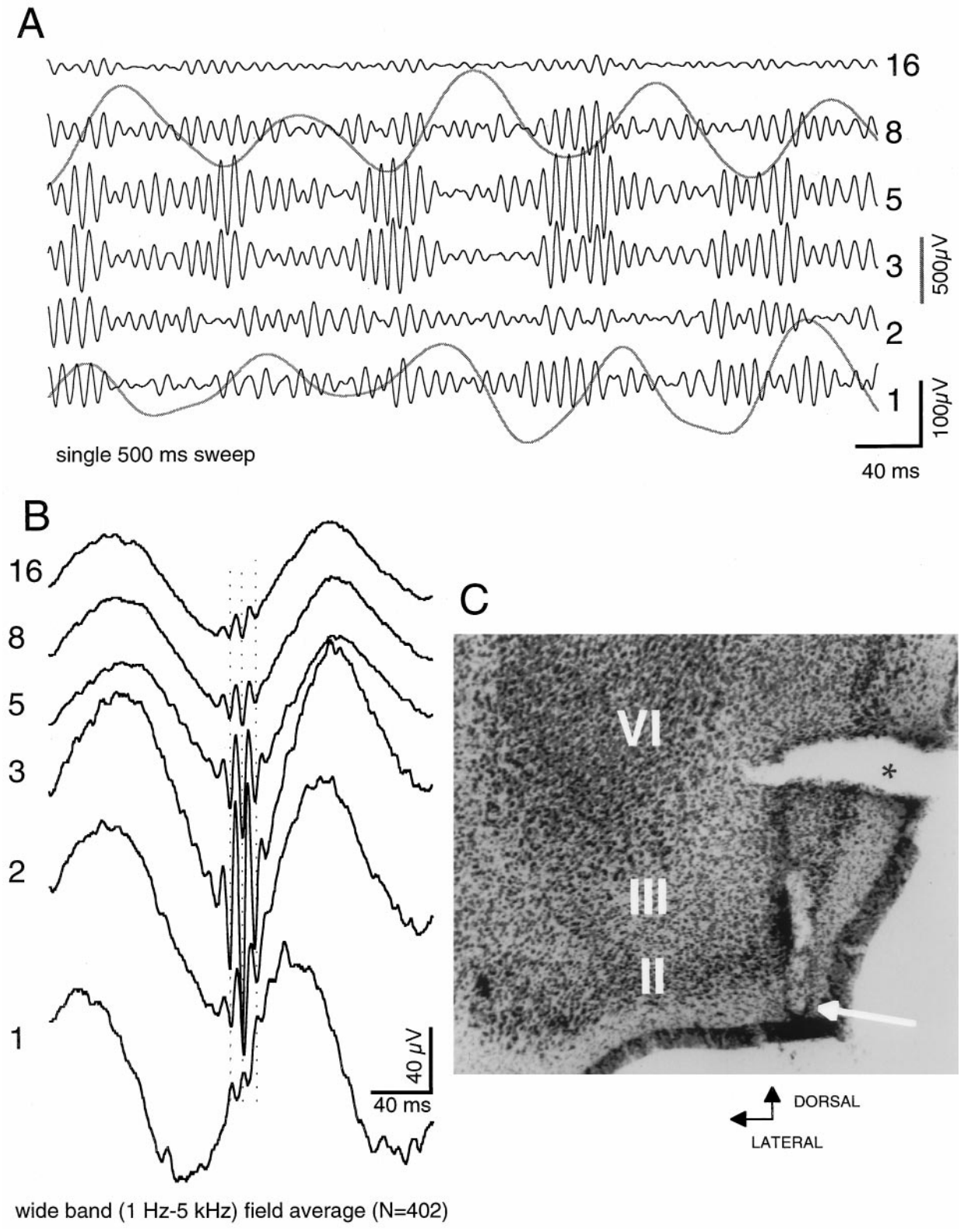

Figure 3. Relation of entorhinal theta to entorhinal gamma. *A*, Single sweep illustrating theta and gamma waves in the entorhinal cortex at six recording positions along the axis of a 16-site recording probe. Six *black traces* are gamma-filtered (50–150 Hz); two *gray traces* show concurrent theta waves (1–20 Hz). *Numerals* at *right* refer to recording positions on silicon probe. Theta records at positions *1* (layer I) and *8* (layer III) are from same sites as gamma traces shown. Note amplitude variation of gamma oscillation at different recording sites. Note also the prominent relation between phase of theta and the amplitude gamma waves. *B*, Averaged ($n = 402$) extracellular field potentials (wide band) as triggered from negative peaks of local gamma oscillation (at site *3*). Note the sudden phase reversal of gamma waves between sites *1* and *2*. *C, arrow*, Recording site 1; *asterisk*, tissue tear.

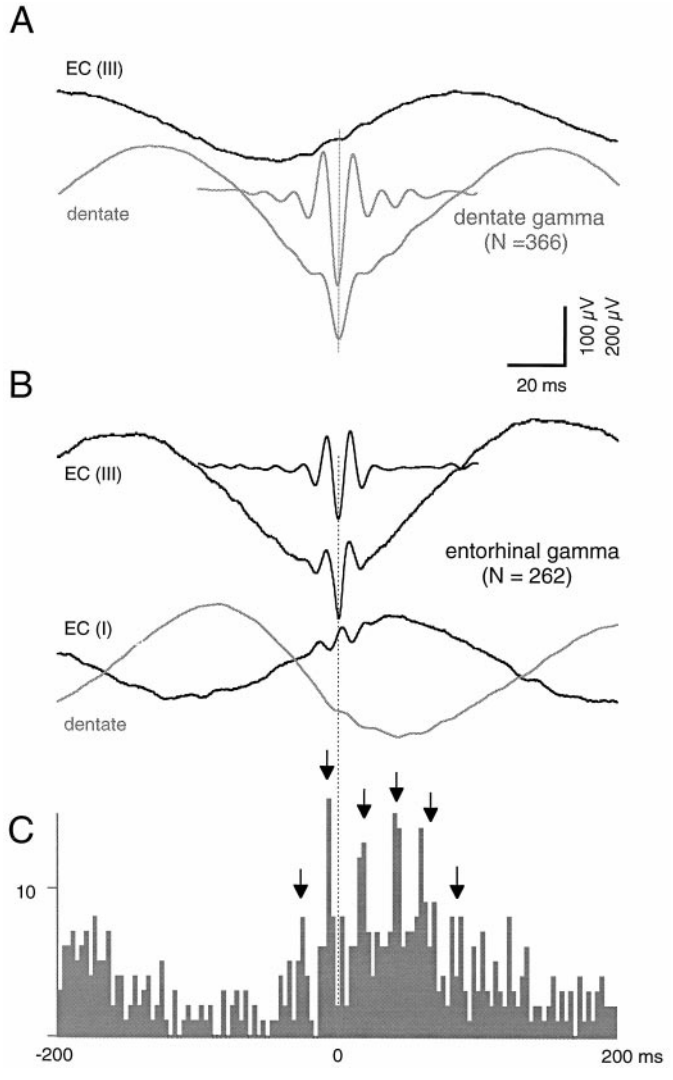

Figure 4. Synchrony between theta and gamma oscillations recorded within layers I–III of caudalateral entorhinal cortex and ipsilateral dentate region. *A*, Averaged field potentials (n = 366) from the dentate hilar region (*gray traces*) and layer III of EC (*black trace*), triggered by negative peaks of dentate gamma oscillation (*short trace*; filtered 50–150 Hz). *B*, Averaged field potentials (n = 262) from EC layers III and I (*black traces*) and ipsilateral dentate hilus (*gray trace*) triggered by negative peaks (layer III) of entorhinal gamma oscillation (*short trace*; filtered 50–150 Hz). *C*, Cross-correlogram between entorhinal gamma waves and dentate gamma oscillation. The *0* (reference) point was the negative peak of filtered layer III gamma waves. *Arrows* point to multiple peaks in cross-correlogram, emphasizing the transient synchronicity in the entorhinal and hippocampal oscillators.

ence observed between any two sites in the entorhinal cortex and hippocampus. Although all sites showed synchrony in the theta range, this varied considerably for gamma.

Superficial layer neurons discharge in relation to local theta and gamma oscillations

We analyzed the discharge characteristics of 31 putative single neurons (as defined by refractory periods of >1.0 msec) and multiunit activity (spikes >100 μV but with refractory periods of <1.0 msec) at 53 sites within layers I–III of the entorhinal cortex (n = 45 penetrations), as well as in the superficial layers of the presubiculum (n = 8) in 19 rats. The majority of single neurons (27 of 31) and multiunit activity (47 of 53) exhibited a peak in the cross-correlogram near the zero reference (±5 msec) point of the local gamma oscillation. All single-unit and multiunit activity in layer II–III was correlated to local field theta waves.

The majority of single neurons fired very slowly (<5 Hz), often exhibiting sustained periods (tens of seconds) of quiescence, although occasionally emitting one to four spikes (typically one) on a sequence of theta cycles. These neurons exhibited varying degrees of modulation for multiple cycles of the gamma oscillation. Typically, putative single neurons exhibited a single prominent peak near the zero reference, minimal firing in the adjacent troughs, and one or two additional broader peaks (Fig. 5). The broadness of the nonzero peaks may result from several factors, including (1) rapid changes in the frequency of the oscillation as it develops and degenerates and (2) the fact that the local field event reflects summation of synaptic potentials over a limited, but ill-defined, area of space. Both of these factors place limitations on detecting and defining the peak of the local field potential, which might reflect synaptic input that contributed to the discharge of any given neuron (for discussion, also see Laurent et al., 1996). One should note that the local field oscillation reflects summation of synaptic input that is constantly varying in time, amplitude, and location. Figure 3 illustrates the amplitude and spatial variation of the local gamma oscillation in filtered traces.

Most neurons exhibited very slow firing rates and discharged irregularly. Figure 5 illustrates the relation of putative single-unit discharges in a single sweep. The unit shown in electrode position 11, for which a cumulative cross-correlogram is also shown (Fig. 5*D*), discharged a single spike during this epoch, as did the unit shown in position 13. Over a 90 sec REM sleep episode, unit 13 discharged at a rate of 3.9 spikes/sec compared with 0.46 spikes/sec for unit 11. These observations illustrate the low probability of concurrent discharge among pairs of layer II–III neurons. Yet, the temporal occurrence of spike discharge in the vast majority of layer II–III neurons was phase-locked to the slow (~125 msec) theta waves and to the associated fast (~10–25 msec) gamma cycles (Fig. 5). These observations indicated that spatially distinct, slowly discharging cells can nevertheless maintain a population oscillation and provide a gamma frequency net excitation to their hippocampal targets. Slowly discharging cells had a relatively wide action potential (>0.6 msec at the base, unfiltered).

Two of 31 single neurons were characterized as fast-spiking cells, emitting sustained firing >20 Hz for long periods (minutes). These two neurons had short-duration action potentials (<0.5 msec, unfiltered). They were strongly theta-modulated and emitted trains of 2–10 action potentials on each theta cycle with quiescence between cycles or exhibiting a relatively sustained firing with their frequency waxing and waning by the phase changes of the local theta cycle (Fig. 6). The discharge of both neurons was phase-related to the local gamma field during both exploratory locomotion and REM sleep. In addition, they were also modulated by the lower-amplitude gamma oscillations present during immobility and slow-wave sleep. Both neurons were located within layer II. On the basis of their distinct physiological features, we tentatively suggest that these fast-firing cells correspond to aspiny stellate interneurons of layer II.

DISCUSSION

During theta waves, associated with exploratory locomotion and REM sleep (Green and Arduini, 1954; Grastyán et al., 1959; Vanderwolf, 1969), neurons within the entorhinal–hippocampal input network discharge in an organized manner (Mitchell and Ranck, 1980; Alonso and Garcia-Austt, 1987a,b; Stewart et al.,

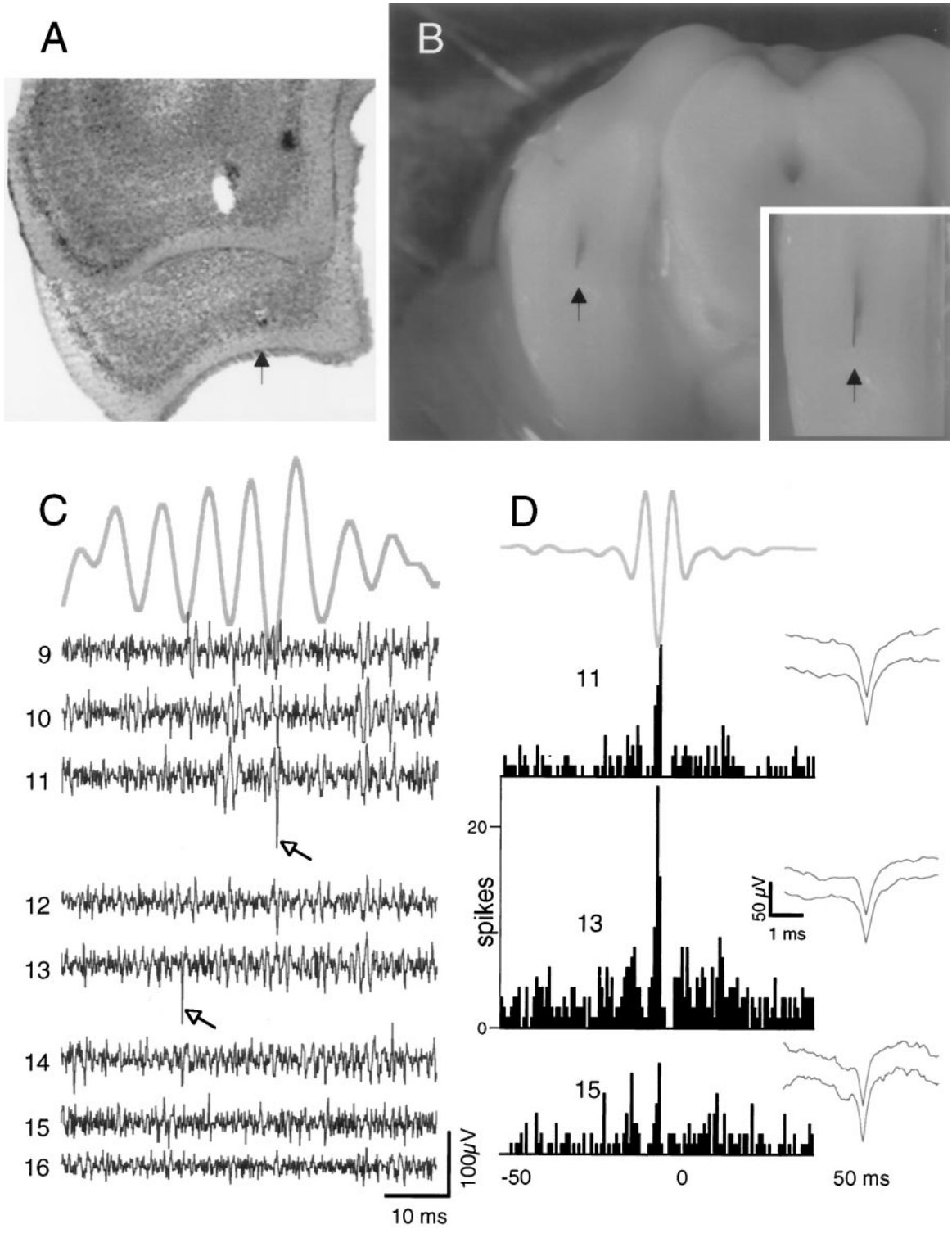

Figure 5. Neuronal activity in layers II and III is phase-locked to gamma waves. *A*, Adjacent Nissl-stained sections illustrating tip of electrode near layer II of the entorhinal cortex taken from brain pictured at *B*. *B*, Silicon probe as it emerges from sectioned rat brain during histological processing. *Inset*, Probe in relation to edge of brain (*arrows* are placed at ventral brain surface). No reversal of gamma oscillation was observed along any of 16 dorsoventral sites along this probe, which recorded from layers II–V of the entorhinal cortex. *C*, Relationship between simultaneously recorded single units and local gamma oscillation, recorded with the lower eight recording sites of the silicon probe in layers II and III. *Arrows* point to two single units (verified by the absence of spikes ≥1 msec in autocorrelograms); a third single unit from site number 15 was also recorded, which did not discharge in trace shown. *Top trace* (from site 13), Single 50 msec gamma wave epoch (50–150 Hz). *Traces 9–16*, Unit filtered traces (0.5–5 KHz). Note prominent single units during this 50 msec sweep in *traces 11* and *13*, as well as their phase relationship to gamma field oscillation. *D*, Cross-correlograms between units *11*, *13*, and *15* (not present in trace shown in *C*) and gamma field oscillation. Note discharge peaks of units in relation to average gamma wave (*top trace*). *Traces* at *right* of each correlogram illustrate unfiltered (wide-band) average of first 30 discriminated waveforms (*top*) and last 30 discriminated waveforms (*bottom*).

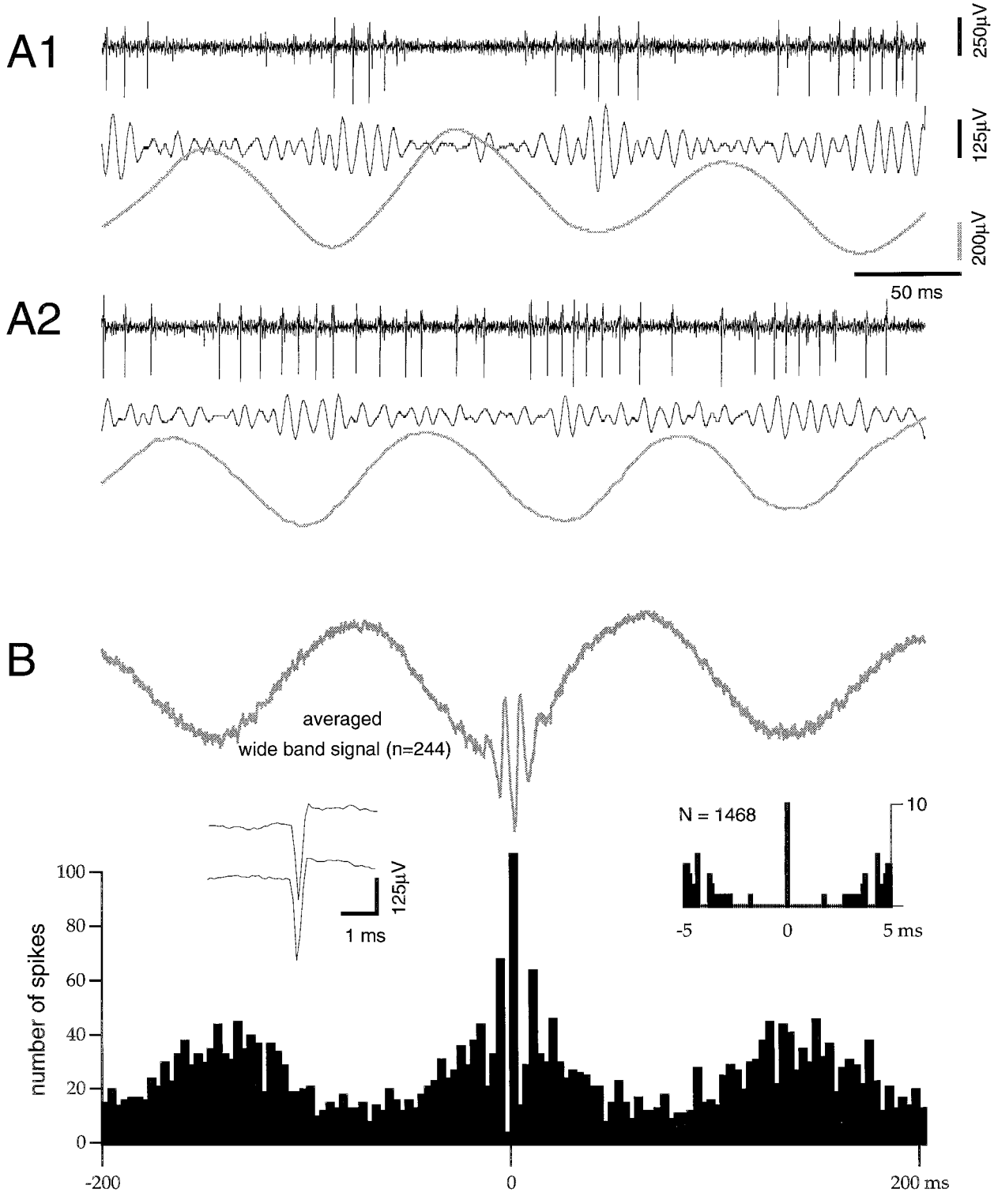

Figure 6. Relationship of putative interneuron of layer II to local theta and gamma oscillations. *A1, A2*, Two 400 msec sweeps from single recording electrode in layer II of the entorhinal cortex. *Top trace* is filtered for unit activity (0.5–5 KHz), *middle* for gamma oscillation (50–150 Hz), and *lower gray trace* for theta (1–20 Hz). Note rhythmic trains of firing in *A1* in association with nested theta–gamma cycles, as well as a more continous discharge pattern in *A2*. *B*, Relationship of single-unit activity to local field gamma oscillation. *Top gray trace*, Average wide-band trace (1 Hz–5 kHz), triggered from negative peak of local gamma oscillation ($n = 244$). *Bottom*, Cross-correlogram showing prominent theta–gamma modulation of unit discharge. *Inset* at *right*, Autocorrelogram of this unit. *Inset*, Unfiltered (1 Hz–5 kHz) average of first 30 discriminated waveforms (*top*) and last 30 discriminated waveforms (*bottom*). Note short duration (<0.5 msec) of the action potential.

1992). Hippocampal and entorhinal neurons are brought together such that they discharge in discrete time windows within the 50–100 msec time frames of a theta wave. The present findings reveal much greater temporal precision in the discharge of layer II–III neurons. Individual layer II–III neurons discharged at a very low rate (<5 Hz), but in phase with local gamma oscillations that occur nested within the theta cycle. Thus, subsets of entorhinal neurons discharge together in 10–25 msec time frames, with varying subsets discharging every 50–100 msec.

The present findings demonstrate that during theta activity a distributed population output, entrained into local gamma rhythms, is fed into the circuitry of the hippocampus. Concurrently, the theta-generating mechanism within the hippocampus brings about a dynamic gamma frequency modulation of hippocampal neurons (Bragin et al., 1995). Previous studies have demonstrated that gamma oscillations in the dentate–hilar region virtually disappear after surgical removal of the entorhinal cortex (Bragin et al., 1995; Charpak et al., 1995).

It is important to recognize that theta–gamma dynamics are not developing equally throughout the entire spatial extent of the network, nor necessarily at fixed frequencies. Rather, transiently synchronized neuronal discharges are emerging within varying topographical locations, involving varying subpopulations of neurons and at a rapidly evolving (but biologically constrained) range of frequencies (Traub et al., 1996; Wang and Buzsáki, 1996). Two issues concerning this variability need to be addressed by subsequent studies. The first issue concerns the variability in the gamma frequency (40–100 Hz). Previous findings concerning the theta–gamma relationship in the dentate–hilar region demonstrate that in this region, gamma frequency varies as a function of theta frequency (Bragin et al., 1995). The results of the present experiments suggest a similar relationship between theta and gamma oscillations in the entorhinal cortex.

The second issue concerns the synchronization of dentate–hilar gamma and entorhinal gamma. In all cases we observed synchronization of gamma oscillations in the theta range (50–100 msec) between sites in the dentate–hilar region and the entorhinal cortex. Synchronization in the gamma frequency varied considerably, although we observed cases in which multiple peaks in the cross-correlogram were evident. In the animal with the most synchronized relationship between any two sites, the electrodes were located in the caudal–lateral aspect of the entorhinal cortex and in the dorsal dentate–hilar region. At least part of the interanimal variability may be accounted for by the specific topographical profile of entorhinal–hippocampal interconnections. Recent findings suggest that there is greater specificity in the anatomical organization of the perforant path input than appreciated previously, with three relatively segregated topographical bands oriented rostrocaudally, innervating three segregated septotemporal domains of the dentate gyrus (D. G. Amaral and C. Dolorfo, personal communication) and fairly circumscribed patches in the CA1 region (Tamamaki and Nojyo, 1995). We suggest that synchrony should vary systematically depending on topographical connectivity, and a systematic mapping of the "physiological connectivity" of this projection, based on a more precise mapping of the anatomical connectivity, warrants further investigation. We predict that synchronization in the gamma frequency range will be a constant feature of the relationship between entorhinal gamma and dentate–hilar gamma, when electrodes are positioned into interconnected domains of the entorhinal–hippocampal axis.

Potential mechanisms

We have demonstrated that gamma oscillations are a feature of the micro-EEG observed in the superficial layers of the entorhinal cortex during theta. Furthermore, the discharge of layer II–III neurons is entrained into a population dynamic in association with the gamma frequency oscillation. How could this dynamic be achieved by local macrocircuits? Within the hippocampus, GABAergic interneurons can produce rhythmic, population discharges in the gamma frequency range. This output then imposes a hyperpolarizing oscillation on the membrane potential of principal neurons (Buzsáki et al., 1983; Soltész and Deschénes, 1993; Bragin et al., 1995; Whittington et al., 1995). The dentate–hilar gamma oscillations thus reflect synchronous membrane oscillations in pyramidal and stellate neurons caused by rhythmic IPSPs (Buzsáki and Chrobak, 1995; Sik et al., 1995; Whittington et al., 1995; Acsády et al., 1996; Freund and Buzsáki, 1996; Gulyás et al., 1996; Traub et al., 1996; Wang and Buzsáki, 1996). Alternatively, recent findings suggest that a specific subclass of cortical pyramidal neurons, "chattering cells," can intrinsically generate gamma frequency discharges on suprathreshold depolarization (Gray and McCormick, 1996). These putative excitatory neurons, observed in layer II–III of both striate and prestriate cortex, could contribute to the generation of gamma band oscillations in those regions. The presence of chattering pyramidal neurons in the entorhinal cortex, however, has yet to be demonstrated.

Inhibition of superficial layer entorhinal cortical neurons, even in the presence of powerful excitatory input, is a consistent feature of this region of cortex (Finch et al., 1986, 1988; Jones and Heinemann; 1988; Jones, 1993; Jones and Buhl, 1993; Chrobak and Buzsáki, 1994). Jones and Buhl (1993) observed a very small percentage of (presumably GABAergic) cells in layer II that were fast spiking (up to 200 Hz) and that extensively arborized in layer II, forming basket-like complexes. A single cell with comparable properties has been described *in vivo* (Tamamaki and Nojyo, 1995). Based on detailed morphological and anatomical analysis of parvalbumin-immunoreactive interneurons in the entorhinal cortex, Wouterlood and colleagues (1995) suggested that the strong inhibitory influence on layer II cells (Jones and Buhl, 1993) was mediated by parvalbumin-positive basket cells. By innervating the perisomatic region of layers II and III, these interneurons would be in a position to generate the synaptic currents observed in the present study. Studies combining *in vivo* intracellular recording and extracellular field recordings would be a powerful means of determining the physiological properties of individual pyramidal neurons and interneurons in the entorhinal cortex, as well as the role of individual neuronal populations to the generation of gamma frequency oscillations.

Possible role of synchrony in neuronal communication and synaptic efficacy

Bringing sparsely firing neurons within the entorhinal cortex together on such a short time scale may provide the requisite means for entorhinal neurons to initiate neuronal discharge at hippocampal targets. A class of fast-spiking interneurons within the dentate gyrus and CA1–CA3 regions as well as other cortical regions is the first to discharge in response to afferent activation and to respond repetitively (Buzsáki and Eidelberg, 1982; Buzsáki, 1984; Llinás et al., 1991; Gulyas et al., 1993). During theta, hippocampal interneurons are entrained into gamma frequency volleys that periodically hyperpolarize the dendritic and somatic compartments of their target cells (Penttonen et al., 1997). The present findings demonstrate that the entorhinal input

is entrained into cooperative oscillatory volleys at the same frequency as the rhythmic hyperpolarization of their hippocampal targets (Bragin et al., 1995). Synchronized excitatory inputs that arrive at the right phase of the rhythmic membrane oscillations may then be able to discharge principal cell targets. Conversely, excitatory potentials arriving out of phase will be less efficient because of the shunting and hyperpolarizing effects of inhibitory potentials at the soma.

The temporal dynamics underlying resonant entrainment of hippocampal neurons may be critically related to the *in vivo* production of synaptic long-term potentiation (LTP) and long-term depression (LTD) (Larson and Lynch, 1986; Rose and Dunwiddie, 1986; Berger and Yeckel, 1991; Huerta and Lisman, 1996). Cooperative activity in the afferent input is a requisite for both LTP and LTD (McNaughton et al., 1978; Bliss and Collingridge, 1993). Huerta and Lisman (1996) have demonstrated the relationship between the phase of population oscillation in the theta range and LTP/LTD (Huerta and Lisman, 1996). The gamma frequency synchronization of the entorhinal output would appear to place faster temporal constraints on the activation and inactivation of membrane currents critical to LTP/LTD.

Conclusions

Gamma frequency synchronization of neuronal activity occurs in virtually all forebrain structures of the mammalian brain. This population pattern is likely to reflect a fundamental operational mode of cortical networks. Synchronization of neuronal populations is often revealed by field oscillations (Gray and Singer, 1989; Bragin et al., 1995; Chrobak and Buzsáki, 1996a; Steriade et al., 1996). The theta–gamma phase locking of principal cells that develop within the entorhinal cortex and hippocampus may provide a basis for effective communication among these neuronal populations.

REFERENCES

Acsády L, Görcs TJ, Freund TF (1996) Different populations of VIP-immunoreactive interneurons are specialized to control pyramidal cells or interneurons in the hippocampus. Neuroscience 73:317–334.

Alonso A, Garcia-Austt E (1987a) Neuronal sources of theta rhythm in the entorhinal cortex of hte rat. I. Laminar distribution of theta field potentials. Exp Brain Res 67:493–501.

Alonso A, Garcia-Austt E (1987b) Neuronal sources of theta rhythm in the entorhinal cortex of the rat. II. Phase relations between unit discharges and theta field potentials. Exp Brain Res 67:502–509.

Amaral DG, Witter MP (1995) Hippocampal formation. In: The rat nervous system, Ed 2 (Paxinos G, ed), pp 443–493. San Diego: Academic.

Berger TW, Yeckel MF (1991) Long-term potentiation of entorhinal afferents to the hippocampus: enhanced propagation of activity through the trisynaptic pathway. In: Long-term potentiation: from biophysics to behavior (Baudry M Davis JL, eds), pp 327–356. Cambridge, MA: MIT.

Bliss TVP, Collinridge GL (1993) A synaptic model of memory: long-term potentiation in the hippocampus. Nature 361:31–39.

Braak H, Braak E (1995) Staging of Alzheimer's disease-related neurofibrillary changes. Neurobiol Aging 16:271–284.

Bragin A, Jandó G, Nadasdy Z, Hetke J, Wise K, Buzsáki G (1995) Gamma (40–100 Hz) oscillation in the hippocampus of the behaving rat. J Neurosci 15:47–60.

Buzsáki G (1984) Feed-forward inhibition in the hippocampal formation. Prog Neurobiol 22:131–153.

Buzsáki G (1989) Two-stage model of memory trace formation: a role for "noisy" brain states. Neuroscience 31:551–570.

Buzsáki G, Eidelberg E (1982) Direct afferent excitation and long-term potentiation of hippocampal interneurons. J Neurophysiol 48:597–607.

Buzsáki G, Chrobak JJ (1995) Temporal structure in spatially organized neuronal ensembles: a role for interneuron networks. Curr Opin Neurobiol 5:504–510.

Buzsáki G, Leung LS, Vanderwolf CH (1983) Cellular basis of hippocampal EEG in the behaving rat. Brain Res 6:139–171.

Buzsáki G, Horváth Z, Urioste R, Hetke J, Wise K (1992) High-frequency network oscillation in the hippocampus. Science 256:1025–1027.

Charpak S, Paré D, Llinás R (1995) The entorhinal cortex entrains fast CA1 hippocampal oscillations in the anaesthetized guinea-pig: role of the monosynaptic component of the perforant path. Eur J Neurosci 7:1548–1557.

Chrobak JJ, Buzsáki, G (1994) Selective activation of deep layer (V-VI) retrohippocampal cortical neurons during hippocampal sharp waves in the behaving rat. J Neurosci 14:6160–6170.

Chrobak JJ, Buzsáki G (1996a) High-frequency oscillations in the output networks of the hippocampal-entorhinal axis of the freely-behaving rat. J Neurosci 16:3056–3066.

Chrobak JJ, Buzsáki G (1996b) Entorhinal-hippocampal network dynamics constrain synaptic potentiation and memory formation. In: Long-term potentiation: current issues (Baudry M, Davies JL, eds), pp 215–232. Cambridge, MA: MIT.

Finch DM, Wong EE, Derian EL, Babb TL (1986) Neurophysiology of limbic system pathways in the rat: projections from the subicular complex and hippocampus to the entorhinal cortex. Brain Res 397:205–213.

Finch DM, Tan AM, Isokawa-Akesson M (1988) Feedforward inhibition of the rat entorhinal cortex and subicular complex. J Neurosci 8:2213–2226.

Freeman W, Barrie F (1994) Chaotic oscillations and the genesis of meaning in the cerebral cortex. In: Temporal coding in the brain (Buzsáki G, Llinás R, Singer W, Berthoz A, Christian Y, eds). Berlin: Springer.

Fregnac Y (1994) Oscillatory neuronal activity in visual cortex: a critical re-evaluation. In: Temporal coding in the brain (Buzsáki G, Llinás R, Singer W, Berthoz A, Christian Y, eds), pp 81–102. Berlin: Springer.

Freund TF, Buzsáki G (1996) Interneurons of the hippocampus. Hippocampus 6:347–470.

Gallyas F, Guldner FH, Zoltay G, Wolff JR (1990) Golgi-like demonstration of "dark" neurons with an argyrophil III method for experimental neuropathology. Acta Neuropathol (Berl) 79:620–628.

Grastyán E, Lissak K, Madarasz I, Donhoffer H (1959) The hippocampal electrical activity during the development of conditioned reflexes. Electroencephalogr Clin Neurophysiol 11:409–430.

Gray CM (1994) Synchronous oscillations in neuronal systems: mechanisms and functions. Comput Neurosci 1:11–38.

Gray CM, Singer W (1989) Stimulus-specific oscillations in orientation columns of cat visual cortex. Proc Natl Acad Sci USA 86:1698–1702.

Gray CM, McCormick DA (1996) Chattering cells: superficial pyramidal neurons contributing to the generation of synchronous oscillations in the visual cortex. Science 274:109–113.

Green JD, Arduini AA (1954) Hippocampal electrical activity in arousal. J Neurophysiol 17:533–557.

Gulyas AI, Miles R Hajos N, Freund TF (1993) Precision and variability in postsynaptic target selection of inhibitory cells in the hippocampal CA3 region. Eur J Neurosci 5:1729–1751.

Gulyás AI, Hájos, N, and Freund TF (1996) Interneurons containing calretinin are specialized to control other interneurons in the rat hippocampus. J Neurosci 16:3397–3411.

Hebb DO (1949) The organization of behavior. New York: Wiley.

Heurta PT, Lisman JE (1996) Bidirectional synaptic plasticity induced by a single burst during cholinergic theta oscillation in CA1 in vitro. Neuron 15:1053–1063.

Hyman BT, Van Hoesen GW, Damasio, AR, Barnes CL (1984) Alzheimer's disease: cell-specific pathology isolates the hippocampal formation. Science 225:1168–1170.

Jones RSG (1993) Entorhinal-hippocampal connections: a speculative view of their function. Trends Neurosci 16:58–64.

Jones RSG, Buhl EH (1993) Basket-like interneurones in layer II of the entorhinal cortex exhibit a powerful NMDA-mediated synaptic excitation. Neuroscience 149:35–39.

Jones RSG, Heinemann U (1988) Synaptic and intrinsic responses of medial entorhinal cortical cells in normal and magnesium-free medium in vitro. J Neurophysiol 59:1476–1496.

Larson J, Lynch G (1986) Induction of synaptic potentiation in hippocampus by patterned stimulation involves two events. Science 232:985–988.

Laurent G (1996) Dynamical representations of odors by oscillating and evolving neural assemblies. Trends Neurosci 19:489–496.

Laurent G, Wehr M, Davidowitz H (1996) Temporal representations of odors in an olfactory network. J Neurosci 16:3837–3847.
Leung LW, Buzsáki G (1983) Spectral analysis of hippocampal unit train in relation to hippocampal EEG. Electroencephalogr Clin Neurophysiol 56:668–671.
Llinás RR (1988) The intrinsic electrophysiological properties of mammalian neurons: insights into central nervous system function. Science 242:11654–11664.
Llinás R, Grace AA, Yarom Y (1991) In vitro neurons in mammalian cortical layer 4 exhibit intrinsic oscillatory activity in the 10- to 50 Hz frequency range. Proc Natl Acad Sci USA 88:897–901.
McNaughton BL, Douglas RM, Goddard GV (1978) Synaptic enhancement in fascia dentata: cooperativity among coactive afferents. Brain Res 157:277–193.
Mitchell SJ, Ranck JB (1980) Generation of theta rhythm in medial entorhinal cortex of freely moving rats. Brain Res 189:49–66.
Murthy VN, Fetz EE (1992) Coherent 25- to 35- Hz oscillations in the sensorimotor cortex of awake behaving monkeys. Proc Natl Acad Sci USA 89:5670–5674.
Pavlides C, Greenstein YJ, Grudman M, Winson J (1988) Long-term potentiation in the dentate gyrus is induced preferentially on the positive phase of theta rhythm. Brain Res 439:383–387.
Paxinos G, Watson C (1986) The rat brain in stereotaxic coordinates, Ed 2. New York: Academic
Penttonen M, Kamondi A, Acsády L, Buzsáki G (1997) Intracellular correlates of hippocampal gamma oscillation in vivo. Soc Neurosci Abstr, in press.
Rose GM, Dunwiddie TV (1986) Induction of hippocampal long-term potentiation using physiologically patterned stimulation. Neurosci Lett 69:244–248.
Sik A, Penttonen M, Ylinen A, Buzsáki G (1995) Hippocampal CA1 interneurons: an in vivo intracellular labeling study. J Neurosci 15:6651–6665.
Singer W (1993) Synchronization of cortical activity and its putative role in information processing and learning. Annu Rev Physiol 55:349–374.
Soltész I, Deschénes M (1993) Low- and high-frequency membrane potential oscillations during theta activity in CA1 and CA3 pyramidal neurons of the rat hippocampus under ketamine-xylazine anesthesia. J Neurophysiol 70:97–116.
Steriade M, Amzica F (1996) Intracortical and corticothalamic coherency of fast spontaneous oscillations. Proc Natl Acad Sci USA 93:2533–2538.
Steriade M, Gloor P, Llinás RR, Lopes da Silva FH, Mesulam M-M (1990) Basic mechanisms of cerebral rhythmic activities. Electroencephalogr Clin Neurophysiol 76:481–508.
Steriade M, McCormick DA, Sejnowski TJ (1993) The sleeping and aroused brain: thalamocortical oscillations in neurons and networks. Nature 262:679–685.
Steriade M, Amzica F, Contreras D (1996) Synchronization of fast (30–40 Hz) spontaneous cortical rhythms during brain activation. J Neurosci 16:392–417.
Steward O, Scoville SA (1976) Cells of origin of entorhinal cortical afferents to the hippocampus and fascia dentata of the rat. J Comp Neurol 169:347–370.
Stewart M, Quirk GJ, Barry M, Fox SE (1992) Firing relation of medial entorhinal neurons to the hippocampal theta rhythm in urethane anesthetized and walking rats. Exp Brain Res 90:21–28.
Tamamaki N, Nojyo Y (1995) Preservation of topography in the connections between the subiculum, field CA1 and the entorhinal cortex in the rats. J Comp Neurol 353:379–390.
Traub RD, Whittington MA, Colling SB, Buzsáki G, Jefferys JGR (1996) Analysis of gamma rhythms in the rat hippocampus in vitro and in vivo. J Physiol (Lond) 493:471–484.
Vanderwolf CH (1969) Hippocampal electrical activity and voluntary movement in the rat. Electroencephalogr Clin Neurophysiol 26:407–418.
Van Hoesen GW, Hyman BT, Damasio AR (1991) Entorhinal cortex pathology in Alzheimer's disease. Hippocampus 1:1–8.
Wang X-J, Buzsáki G (1996) Gamma oscillation by synaptic inhibition in an interneuronal network model. J Neurosci 16:6402–6413.
Whittington MA, Traub RD, Jefferys JGR (1995) Metabotropic receptor activation drive synchronized 40 Hz oscillations in networks of inhibitory interneurons. Nature 373:612–615.
Wise KD, Najafi K (1991) Microfabrication techniques for integrated sensors and microsystems. Science 254:1335–1342.
Witter MP, Groenewegen HJ (1984) Laminar origin and septotemporal distribution of entorhinal and perirhinal projections to the hippocampus in the cat. J Comp Neurol 224:371–385.
Wouterlood FG, Hartig W, Bruckner G, Witter MP (1995) Paravalbumin-immunoreactive neurons in the entorhinal cortex of the rat: localization, morphology, connectivity and ultrastructure. J Neurocytol 24:135–153.
Ylinen A, Sik A, Bragin A, Nadásdy Z, Jandó G, Szabó I, Buzsáki G (1995) Sharp wave-associated high-frequency oscillation (200 Hz) in the intact hippocampus: network and intracellular mechanisms. J Neurosci 15:30–46.